10TH INTERNATIONAL SYMPOSIUM ON PARTICLE IMAGE VELOCIMETRY – PIV13
Delft, The Netherlands, July 2-4, 2013

μPIV study of droplet fission in a bifurcating microchannel

Chen-li Sun[1] and Sheng-Long Liu[2]

[1] Department of Mechanical Engineering, National Taiwan University, Taipei, Taiwan
clsun@ntu.edu.tw

[2] Department of Mechanical Engineering, National Taiwan University of Science and Technology, Taipei, Taiwan

ABSTRACT

In this study, we exploit the μPIV (microscale particle image velocimetry) analysis to investigate the internal flow field of a dividing droplet in a bifurcating microchannel. Herein, droplets are generated by a flow focusing scheme and sent downstream toward an asymmetric bifurcation. In order to control the proportion of split droplets, we design the lengths and widths of the two arms such that the ratio of the flow resistances conforms to the designate values and pressure drops are equalized across the two daughter channels. During the experiments, three bifurcation angles (θ = 30°, 60°, 180°) and four flow resistance ratios (R_1/R_2 = 0.01, 0.13, 0.38, 0.62) are considered. Similar to the results reported by previous literatures, a pair of counter-rotating recirculation is formed inside the droplet that travels along the mother channel in order to roll against the walls. When the droplet approaches the bifurcation of θ = 30° or 60°, however, the presence of the pinnacle break up the two vortices and a saddle point emerges. Once the interface of the droplet touches the vertex of the bifurcation, fluid tends to be pulled into the wider branch because of smaller capillary pressure needed. As a result, the saddle point shifts toward the wider branch and eventually the sharp edge of the bifurcation snap off the end cap of the droplet. Once the fission is complete, flows inside the two daughter droplets gradually retrieve back to the normal rolling configuration as they travel downstream. For the bifurcation of θ = 180°, however, the droplet monotonically slows down when it approaches the T branch. The opposite two arms pull the droplet apart more evenly without the aid of a sharp edge and the saddle point remains close to the stagnation point during the fission process. We find that the size ratio of the two daughter droplets is less extreme for θ = 180° and they nearly move in the same speed after the fission.

INTRODUCTION

To facilitate lab-on-a-chip, precise control over droplet size and reagent concentration in droplet-based microfluidics is essential. The actions of droplet fission and coalescence offer an alternative for pipetting and dilution that are so commonly used in chemical and biological laboratories. In a continuous-flow scheme, the most common way to break a droplet is using a bifurcating T-junction [1-4]. A preliminary study of Tan, et al. [5] in 2003 examined the influence of splitting angle and downstream channel width in droplet fission process. Later, Tan, et al. [5] found that there existed a critical capillary number above which droplet fission occurred. This conclusion was also verified by the work of Link, et al. [3]. Tan, et al. [5] also found that the critical capillary numbers were relatively large when bifurcation was either too wide or too narrow. A bifurcation angle of 90° resulted in the lowest critical capillary number, suggesting that droplet was more easily split with θ = 90°. Ménétrier-Deremble and Tabeling [6] studied droplet breakup in microfluidic junctions of various angles. Characterized by the critical length that depended on the junction angle, the breakup process was classified into two regimes: direct breakup and retarded breakup. Nevertheless, Ménétrier-Deremble and Tabeling [6] did not reveal any information regarding to the sizes of the splitting droplets. Tan et al. [1] suggested that the volume of daughter droplets depended on both the resistance of the channels and the size of the mother droplet. According to Link, et al. [3], the relative size of the daughter droplets was inversely proportional to lengths of the two arms if the channel widths were fixed. Nei and Kennedy [2] implemented asymmetric splitting of droplet by using T-junction with branches of different lengths and identical width. A split ratio as high as 34:1 was accomplished. To prevent downstream droplet accumulation from interfering with the fission process, Nei and Kennedy [2] looped the downstream channel of an asymmetrical T-junction to equalize pressure. Small posts were added to separate the droplets, but continuous phase was allowed to cross. From the experimental results, Nei and Kennedy [2] found that the split ratio depended not only on dimensions of downstream channels but also on frequency of plugs. Different kinds of asymmetric bifurcations were studied by Bedram and Moosavi [7] numerically using a volume of fluid (VOF) method. With the same length but different widths, Bedram and Moosavi [7] found that branches of closer size reduced the breakup length and decreased the pressure drop. Later, Samie, et al. [8] carried out an experimental investigation to study the volume ratio and breakup point for T-microchannel with branches of the same length but different widths. They found out the optimization of droplet fission in T-junction was achieved by branches with more comparable widths and low capillary number flows.

Several researchers have focused on studying the mechanisms of droplet breakup in a symmetric T-microchannel. Garstecki, et al. [9] suggested that the dominant effect in droplet breakup was the balance of hydrostatic pressures across interface. This pressure drop came from the squeezing mechanism that was caused by the push of the continuous fluid and channel blockage of the disperse fluid. While droplet did experience a linear squeezing at its early stage, the μ-PIV study of van Steijn et al. [10, 11] revealed that the pinch-off was actually triggered by a sudden flow of continuous fluid through the gap of the neck. Leshansky and Pismen [12] speculated that the droplet breakup was rather flow driven. Leshansky and Pismen [12] used lubrication theory to construct a model that analyzed flow in the narrow gap between droplet and channel wall. By joining the concave and convex arcs of the interface, a critical capillary number was derived for a fixed droplet volume. Jullien, et al. [13] categorized the breakup process into two regime: obstructed and nonobstructed. In the obstructed regime, droplet blocked the T-junction throughout the breakup process and squeezing occurred. In the nonobstructed regime, on the other hand, a gap existed between the droplet and the wall and caused tunneling effect during the breakup. Similar observation was made by Fu, et al. [14] for bubble breakup in a symmetric T-microchannel. Nevertheless, breakup mechanisms in an asymmetric bifurcation remain unexplored albeit its complex phenomena involved. To address this need, this study aims at studying the droplet breakup process in an asymmetric bifurcating microchannel with different angles and branch widths. We use μPIV technique to facilitate measurements of flow field inside a dividing droplet. Since downstream condition may interfere with the fission process [4, 15, 16], we design the bifurcating microchannel with separate outlets to eliminate the feedback effect. Based on the flow resistance calculation, the lengths of the branches are adjusted such that pressures at the two outlets are equalized. Under various flow rates, we investigate the influences of two geometrical factors: bifurcation angle and flow resistance ratio of branches. From the μPIV results, different types of deformation rate are determined for disperse fluid during the breakup process to shed light on the fission mechanisms. The outcome proves to be beneficial to future design of an asymmetric fork for precise control over splitting droplets.

EXPERIMENTAL SETUP

The bifurcating microchannel and the schematic of experimental setup are illustrated in Fig. 1. Two syringe pumps (kdScientific, kds210) are employed to deliver the continuous-phase fluid (silicone oil, Wacker-Chemie, AK10) and disperse-phase fluid (distilled water, Nang Kuang Pharmaceutical). The flow rate of the disperse phase $\dot{Q}_d$ is set to 0.1 ml min^{-1}, while the continuous phase flows through each inlet ($\dot{Q}_c$ / 2) at a flow rate varying from 0.04 ml min^{-1} to 0.14 ml min^{-1}. The internal flow field inside the droplet during its fission process is studied by μPIV diagnosis. The μPIV system is composed of an inverted microscope (DM-IRM, Leica) with a 5X objective (N PLAN, Leica, NA = 0.12), a CMOS high-speed digital camera (MotionPro X3, IDT vision), and a personal computer equipped with camera control software (MotionPro X Studio, IDT vision). To provide illumination, a 100 W halogen lamp is placed above the inverted microscope in a backlighting arrangement. The frame rate of the high-speed camera is set to 6,040 fps with a 15 μs exposure time. The PIV processing is done by PIVLab [17] and mask is activated so that only region of interest (droplet) is evaluated. The size of the interrogation windows is set to 10 × 10 pixels, which corresponds to a grid spacing of 39 × 39 μm. The disperse-phase fluid is seeded with polyamide particles (Dantec dynamics, density = 1,030 kg m^{-3}) of 5 μm in diameter. The corresponding relaxation time is 1.19 μs in water, and the volume ratio of microspheres to fluid is in the range of 0.4-0.5% so that each interrogation window contains approximately 7-8 microspheres. Besides PIV measurements, the size and centroid velocity of droplets are calculated by ImageJ [18]. Relative velocities of the flow field are then determined by subtracting the centroid velocity of the droplet from the μPIV results. We also install two pressure transducers (Validyne, DP103) to the outlets of the bifurcating microchannel. With a demodulator (Validyne, CD23), a data acquisition card (Adlink, DAQ-2214) and a computer, dynamic pressures are recorded at an acquisition rate of 1 kHz. When pressure measurement starts, the labVIEW (National Instruments) program sends a TTL signal to the high-speed camera to trigger the recording event so that image acquisition is synchronized.

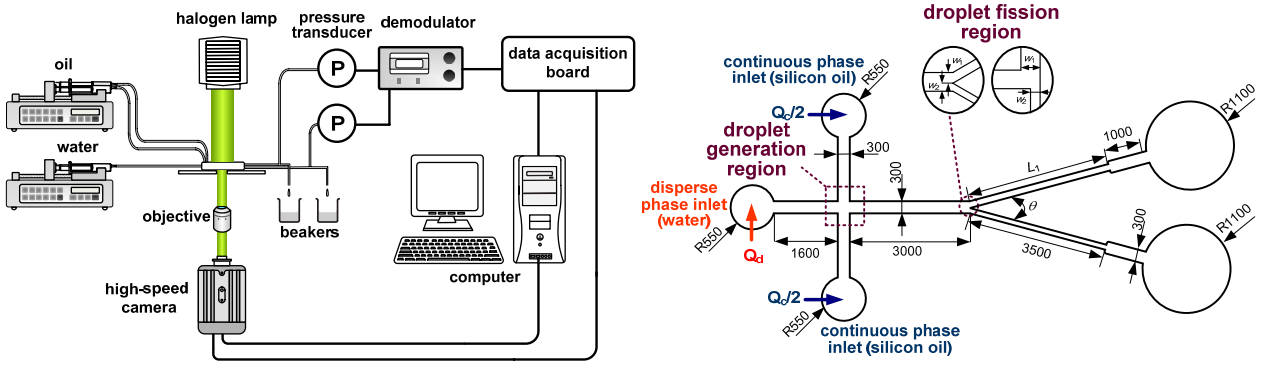

(a) (b)

Figure 1 (a) schematic of experimental setup (b) depiction of bifurcating microchannel, unit: μm.

As shown in Fig. 1 (b), the bifurcating microchannel consists of a cross-flow region for droplet generation, a mother channel, and a bifurcation region that connects the two daughter channels. The feed ducts are all 1600 μm long and 300 μm wide, and the mother channel is 3,000 μm long and 300 μm wide. We design the bifurcating microchannel with three different bifurcation angles (θ = 30°, 60°, 90°) that evenly separates the two daughter channels. The length of the narrower fork is fixed to 3,500 μm and the sum of w_1 and w_2 is kept at 300 μm. By equating the pressure drops across the two forks, we can calculate the widths of the two daughter channels w_1 and w_2 for a given flow resistance ratio R_1/R_2. The flowchart of the determination of w_1 and w_2 is depicted in Fig. 2.

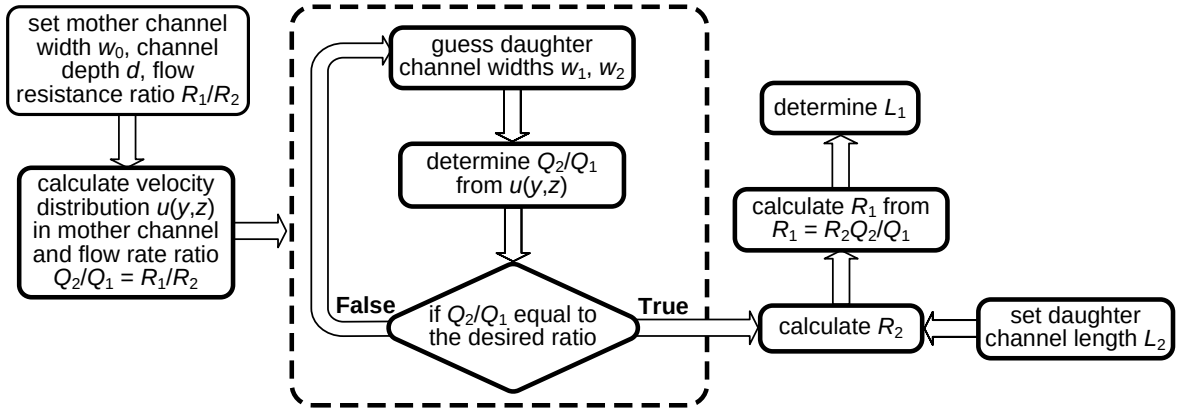

Figure 2 Flowchart to determine the dimensions of the daughter channels.

For a given width w_0 and depth d, the velocity profile in the mother channel can be expressed as [19]:

$$u(y,z) = -\frac{4{w_0}^2}{\mu_c \pi^3}\nabla P \sum_{n=1,3,5...}^{\infty} (-1)^{(n-1)/2}\left[1-\frac{\cosh(n\pi z/w_0)}{\cosh(n\pi d/2w_0)}\right]\cdot\frac{\cos(n\pi y/w_0)}{n^3} \quad (1)$$

where ∇P is the pressure gradient across the mother channel and μ_c is the viscosity of the continuous phase. Assuming that fluid flow retains the same velocity profile at the bifurcation, the ratio of the volumetric flow rates in the daughter channels $\dot{Q}_1/\dot{Q}_2$ can be calculated from:

$$\frac{\dot{Q}_1}{\dot{Q}_2} = \frac{\int_0^d\int_0^{w_1} u(y,z)dydz}{\int_0^d\int_{w_1}^{w_1+w_2} u(y,z)dydz} \quad (2)$$

If we assume the pressure drops across the daughter channels are identical, the ratio of flow resistance R_1/R_2 should be the reciprocal of $\dot{Q}_1/\dot{Q}_2$. Once R_1/R_2 is known, we are able to determine w_1 and w_2 by matching $\dot{Q}_1/\dot{Q}_2$ iteratively. Because L_2 is fixed at 3,500 μm in our design, we can calculate R_2 accordingly and R_1 is equal to $R_2\dot{Q}_2/\dot{Q}_1$. The flow resistance of the daughter channel R_i is given by:

$$R_i = \frac{12\mu_c L_i}{\max(w_i,d)^3\min(w_i,d)}\left[1-\frac{192\max(w_i,d)}{\pi^5\min(w_i,d)}\sum_{n=1,3,5}^{\infty}\frac{\tanh(n\pi\min(w_i,d)/2\max(w_i,d))}{n^5}\right]^{-1} \quad (3)$$

From Eq. (3), we can determine L_1 once R_1 is known. In this study, the flow resistance ratio R_1/R_2 is set to 0.01, 0.13, 0.38, and 0.62. All the geometric parameters are summarized in Table 1. The microdevices are fabricated from PDMS (polydimethylsiloxane) blend (RTV615, GE Silicones) by the standard SU8 (SU-8 2150, MicroChem) molding method. The depth of the microchannels d is 153.5 μm.

Table 1 geometric parameters of the bifurcating microchannels

bifurcation angle θ	30°, 60°, 180°			
flow resistance ratio R_1/R_2	0.62	0.38	0.13	0.01
daughter channel width w_1	171	190	216	254
daughter channel width w_2	129	110	84	46

RESULTS AND DISCUSSION

Fig. 3 illustrates the effects of flow rate ratio of continuous to disperse phase $\dot{Q}_c/\dot{Q}_d$ on droplet fission in the bifurcating microchannels of various R_1/R_2. We find that droplet cannot be divided successfully if the ratio of flow resistance R_1/R_2 and the flow rate ratio $\dot{Q}_c/\dot{Q}_d$ are too low. In the bifurcating microchannel of θ = 30° or 60°, droplet fission is only observed for $R_1/R_2 \geq 0.38$ and $\dot{Q}_c/\dot{Q}_d \geq 0.8$. When the difference between flow resistances R_1 and R_2

becomes too great (small R_1/R_2), capillary force exerts a large resistance in the narrower channel and the incoming droplets pass through the wider channel without fission. In the bifurcating microchannels of $R_1/R_2 \geq 0.38$, on the other hand, the first droplet breaks up successfully but the narrower channel is then blocked by the daughter droplet and continuous fission is not possible. We call this phenomenon 'wetting blockage.' When $\dot{Q}_c / \dot{Q}_d$ is small, both mother droplet and dividing droplet in the narrower channel are long such that droplets have large contact area with the channel walls. Therefore, the momentum provided by the continuous-phase fluid flow is not sufficient to drive the long droplet in the daughter channel at low $\dot{Q}_c / \dot{Q}_d$. As $\dot{Q}_c / \dot{Q}_d$ increases, droplets become smaller and driven momentum augments as well. When $\dot{Q}_c / \dot{Q}_d$ exceeds 0.4, droplet is successfully divided by the bifurcating microchannel of $R_1/R_2 \geq 0.38$ for θ = 30° and 60°. For a bifurcation angle of 180°, similar phenomena are observed. However, we notice that droplet fission is only achieved within $0.8 \leq \dot{Q}_c / \dot{Q}_d \leq 2$ if the resistance ratio is equal to 0.38. Two factors may contribute to the failure of droplet fission for $\dot{Q}_c / \dot{Q}_d > 2$. Without the pinching effect from the sharp corner at the bifurcation, droplet breakup solely depends on the stretches of fluid flows in the two arms. While higher $\dot{Q}_c / \dot{Q}_d$ produces smaller mother droplets that require higher shear stresses to split, the width of the narrower channel deceases with the reduction of R_1/R_2. As a result, the combination of larger capillary resistance of daughter channnel and stronger interfacial effect prevents droplets from fragmentation and pass onto the wider channel directly for $\dot{Q}_c / \dot{Q}_d > 2$ in the bifurcating microchannel of R_1/R_2 = 0.38 and θ = 180°. We also notice that droplet fission always leave a satellite drop behind for bifurcation of 180°, suggesting that its fission mechanism may be different from that of θ = 30° or 60°.

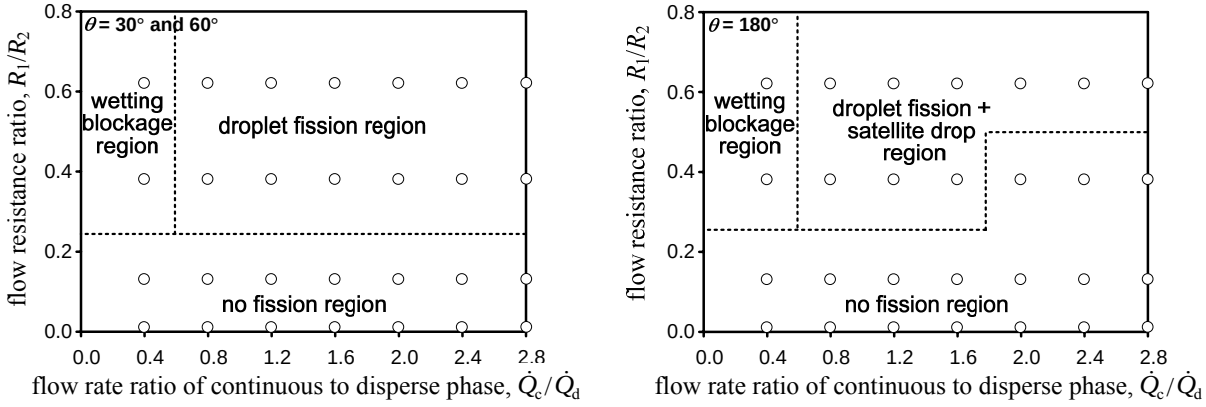

Figure 3 Influences of flow rate ratio of continuous to disperse phase in droplet fission by the bifurcating microchannel of various flow resistance ratio, (a) θ = 30° and 60°, (b) θ = 180°.

Figure 4 compares the sizes and ratios of the daughter droplets in various bifurcating microchannels. From Fig. 4 (b), we find that bifurcating microchannel of R_1/R_2 = 0.38 always leads to higher area fraction of splitting droplets A_1/A_2. This is because difference in flow resistances of the two forks becomes greater at lower R_1/R_2, resulting in daughter droplets with highly disproportional sizes. According to Fig. 4 (a), the influence of flow resistance ratio in droplet size is particularly evident in the narrower channel. We find that bifurcating microchannels of R_1/R_2 = 0.38 produce slightly larger droplets in the wider fork (higher A_1), but much smaller droplets in the narrower fork (lower A_2). As a result, A_1/A_2 can reach as high as 17.4 for R_1/R_2 = 0.38 and θ = 60°. When the flow resistance ratio is 0.62, on the other hand, the resultant A_1/A_2 is always below 6.2 for all bifurcation angles. Moreover, the bifurcation angle plays a more complex role in the sizes of daughter droplets. Regardless of the flow resistance ratio, a bifurcation angle of 180° tends to produce droplets of more comparable sizes that lead to the lowest A_1/A_2. For θ = 30° and 60°, the impact of the bifurcation angle is less straightforward. As the bifurcation becomes more asymmetric with lower R_1/R_2, the role of the capillary forces is accentuated. Because a bifurcation angle of 60° leads to the narrowest w_2, interfacial tension slows down the fluid flows in the narrower branch and the corresponding droplets are quite small for θ = 60°. When the size difference of the two branches is lessen, the overall flow resistance affects both the droplet generation and droplet fission process. Hence, a bifurcation angle of 30° leads to the smallest mother droplet and the tiniest daughter droplets in both branches. In general, we find that the values of A_1/A_2 are dominated by the droplet size in the narrower channel A_2. The highly unequal proportions of droplets created by the asymmetric bifurcation prominences the role of A_2. In contrast, the influence of $\dot{Q}_c / \dot{Q}_d$ in A_1/A_2 is monotonic. We find that area fraction of daughter droplets A_1/A_2 increases with the reduction of flow rate ratio $\dot{Q}_c / \dot{Q}_d$. Because lower $\dot{Q}_c / \dot{Q}_d$ results in smaller capillary number *Ca*, interfacial forces dominate and mother droplets experience longer deformation before splitting up. Therefore, the sizes of two daughter droplets are less equivalent and A_1/A_2 heightens. In fact, the droplet fission process is not very stable for θ =

30° and 60° at low $\dot{Q}_c / \dot{Q}_d$. For $\dot{Q}_c / \dot{Q}_d$ = 0.8 and 1.2, the sizes of the splitting droplets may change in time, suggesting that the fission process is subject to the pressure fluctuation downstream. Because the daughter droplets in the narrower channel are always smaller, this impact is particularly severe and the variation in A_2 is quite noticeable.

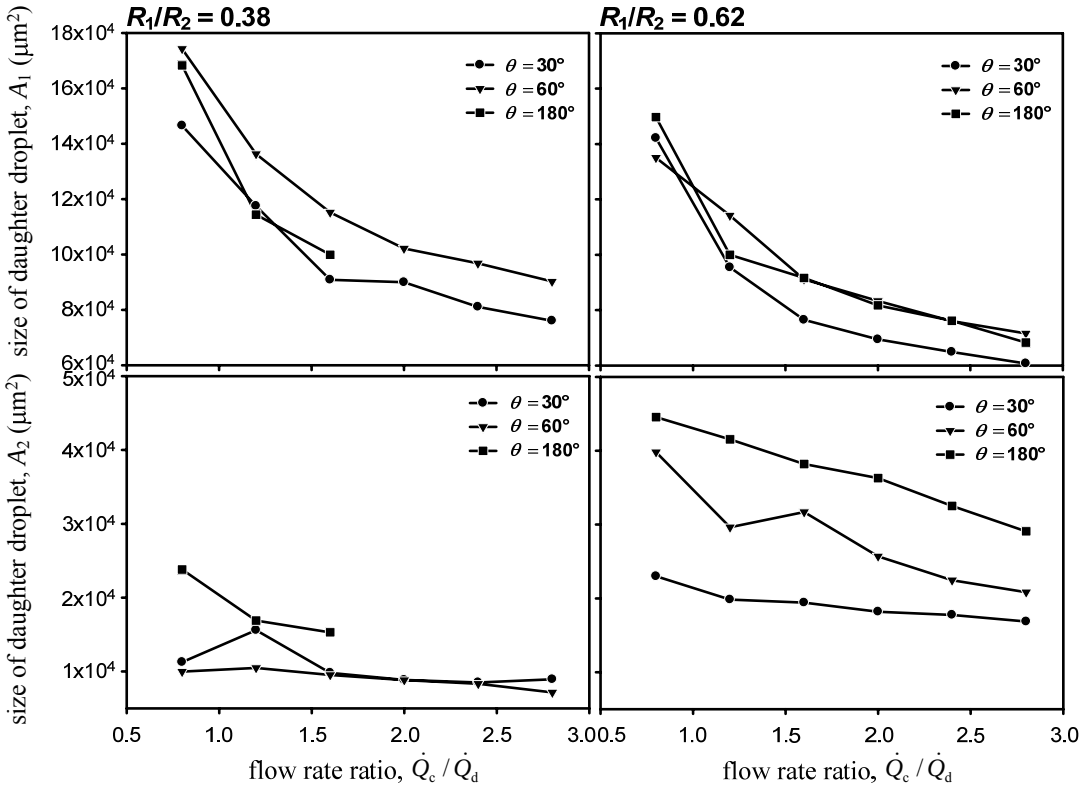

Figure 4 Influences of flow rate ratio of continuous to disperse phase in (a) sizes and (b) area fraction of splitting droplets.

According to the aforementioned observation, the fission processes are quite different for θ = 180° in comparison of those for θ = 30° or 60°. Without the sharp corner at the bifurcation, droplet fragmentation is initiated by the necking phenomena. The incoming flow pushes the smooth interface to bend inward gradually and eventually the droplet snaps off. This concave deformation only occurs for a bifurcating microchanel of θ = 180°. For θ = 30° or 60°, mother droplets are more likely being split by the sharp corner at the bifurcation. To further examine the mechanism of droplet fission, we utilize the μPIV diagnosis to measure the flow field inside the droplet during its fragmentation process. We also estimate the centroid velocity of the droplet spontaneously such that the relative flow with respect to the motion of the droplet is investigated. When $\dot{Q}_c / \dot{Q}_d$ is set to 2, the results during droplet fission in a bifurcating microchannel of θ = 30° and R_1/R_2 = 0.62 are shown in Fig. 5. Similar to previously mentioned in literature [20], a pair of counter-rotating recirculation forms inside the droplet to roll against the walls when droplet travels along the mother channel. As the

droplet approaches the bifurcation, however, the front slows down and the two vortices break up. From Fig. 5, we find that a saddle point emerges inside the droplet from 0 to 1.162 ms. When the droplet touches the vertex of the bifurcation, fluid near the front cap is drawn toward the wider branch and the interface starts to deform. This is ascribed to the lower pressure drop between the hemispherical cap of the droplet and the surrounding thin film in adjacent to the wider channel [21]. Since fluid flows faster in the wider channel, the droplet accelerates accordingly which shifts the saddle point toward the wider branch. As a result, fluid is repelled away from the sharp corner and the narrower channel with respect to the motion of the droplet. When a large portion of the droplet advances into the wider channel, the saddle point gradually disappears. Right before the rear cap is cut by the pinnacle, most fluid flows backward with respect to the droplet. At t = 3.154 ms, a source appears in proximity of the advancing front in the wider channel and emanates forward streamlines toward a sink downstream. Finally, this onward flow pulls the droplet going until the rear cap is snapped off by the sharp edge of the bifurcation. Due to the acceleration of flow in the wider channel, the daughter droplet in the wider branch is much larger than that in the narrower branch. Once the droplet fission is complete, flows inside the two daughter droplets gradually retrieve back to the normal rolling configuration as they travel downstream.

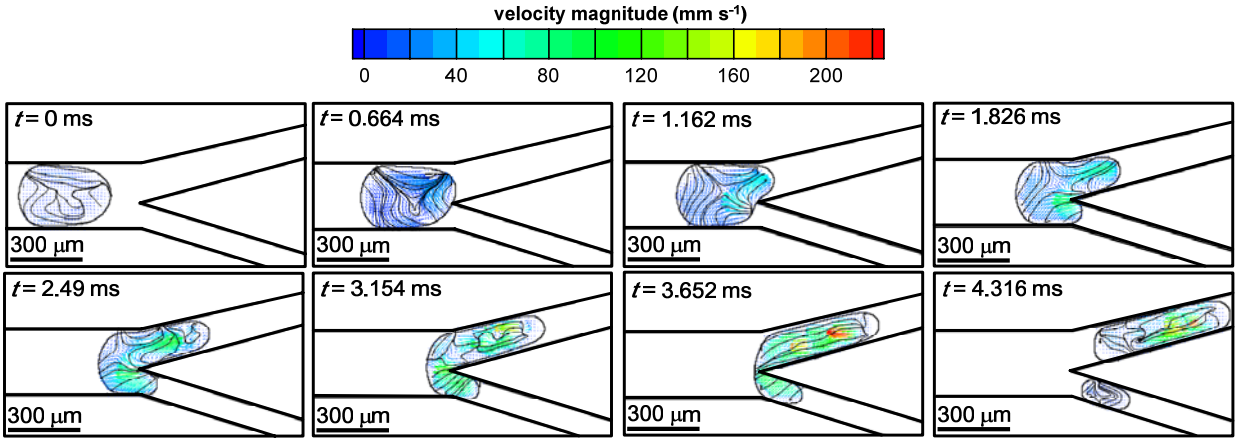

Figure 5 relative velocities inside the dividing droplet in the bifurcating microchannel of $R_1/R_2 = 0.62$ and $\theta = 30°$, $\dot{Q}_c / \dot{Q}_d = 2$.

Figure 6 shows various types of deformation rate in droplet during the fission process in a bifurcating microchannel of $R_1/R_2 = 0.62$, $\theta = 30°$. When the droplet touches the sharp corner at t = 1.826 ms, rate of linear deformation reaches as high as 5400 s^{-1} near the droplet cap in the narrower channel and fluid near the droplet cap in the wider channel experiences a rate of linear deformation around -1800 s^{-1}. Hence, fluid is severely stretched near the front interface in the smaller branch and squeezed near the cap in the larger branch. From Fig. 6 (b), the moderate strain rates near the outer walls of the branches also reveal that fluid experiences angular deformation when flowing through the inclined walls of the bifurcation. In the wider channel, the vorticity is relatively large near the pinnacle and the outer sidewall. The opposite signs of vorticities in these two regions suggest that a pair of counter-rotating circulation emerges inside this portion of the droplet that is pulled into the wider channel. At the early stage of droplet fission, the tip of the droplet is drawn into the narrower channel while fluid in the wider channel tries to resume the rolling motion that leads to compression near the cap due to stagnation. The presence of the pinnacle results in strong rotation of fluid. Moreover, droplet is skewed when it enters the two branches due to the geometry of the bifurcation. At t = 3.154 ms, fluid flow in the wider branch forms a source-sink pair where high rates of deformation are discovered. At this later stage of droplet fission, no significant stretch of fluid is found in the narrower channel. Instead, fluid experiences high angular deformation near the joint of the smaller branch and the inner sidewall of the pinnacle. In the wider branch, rotation is enhanced near the pinnacle.

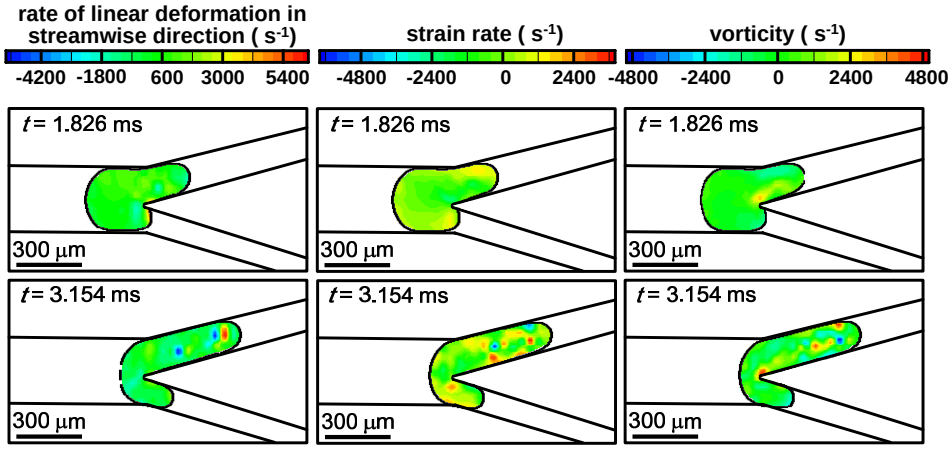

(a) (b) (c)

Figure 6 deformation rate for $R_1/R_2 = 0.62$, $\theta = 30°$ and $\dot{Q}_c / \dot{Q}_d = 2$ during the fission process, (a) rate of linear deformation in the streamwise direction, (b) strain rate, and (c) vorticity

For $\theta = 180°$, in contrast, no acceleration is observed and the droplet monotonically slows down when it approaches the T branch. Figure 7 exhibits the evolution of the relative velocity field inside the droplet during its fission process in a bifurcating microchannel of $\theta = 180°$ and $R_1/R_2 = 0.38$. Similarly, two counter-rotating vortices roll against the walls when the droplet travels along the mother channel. As the droplet enters the fission region, the existence of the perpendicular wall slows down the droplet and disarranges the two vortices inside. According to Fig. 7, a saddle point is present inside the droplet from 0.83 ms to 2.324 ms. We also find that the droplet is solely stretched toward the wider channel, while streamlines in the rear portion of the droplet point toward the narrower channel. Unlike the results of 30° and $R_1/R_2 = 0.62$, the interface is not pulled into the narrower channel until only a small portion of the droplet is left in the mother channel. At $t = 2.988$ ms, we notice that the flow field inside the droplet is under reconfiguration such that fluid starts to flow in opposite direction. Starting from $t = 3.818$ ms, the interface experiences the impingement of the continuous-phase fluid flow from the mother channel and starts to curve inward. This leads to the necking of the droplet and eventually the droplet splits. At $t = 4.98$ ms, the interface recoils and two droplets travel separately in the daughter channels. Right after the fragmentation, a satellite droplet is left near the stagnation point and passes on to the wider channel as time proceeds. Without a sharp edge at the fission region, droplet fission is completed by the pulling of fluid flows in the two arms for $\theta = 180°$. The saddle point remains close to the stagnation point during the process. In contrast to the bifurcation angle, we find that flow resistance ratio does not play a vital role in the evolution of flow field inside the droplet during the fission process.

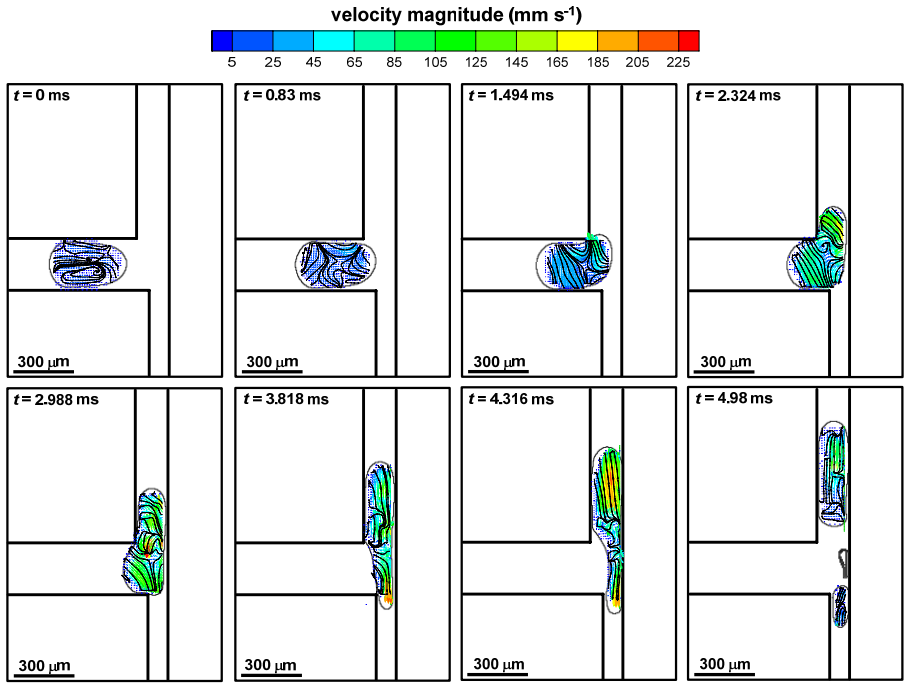

Figure 7 relative velocities inside the dividing droplet in the bifurcating microchannel of $R_1/R_2 = 0.38$ and $\theta = 180°$, $\dot{Q}_c / \dot{Q}_d = 2$

Figure 8 exhibits the rate of linear deformation of fluid inside the droplet at t = 4.316 ms. We find that the stretching rate in the y direction is much larger than that in the x direction. Because of the incoming flow, positive and negative $\partial u/\partial x$ are found near the left and right side of the necking region, suggesting that the neck of the droplet is squeezed during the pinch-off process. On the other hand, the regions with high rate of linear deformation in the y direction appear at the stems and tips of the dividing droplet. While positive $\partial v/\partial y$ suggests that disperse-phase fluid is stretched toward the two arms near the entrances of the daughter channels, the negative $\partial v/\partial y$ near the caps indicates fluid is compressed in adjacent to the front interfaces.

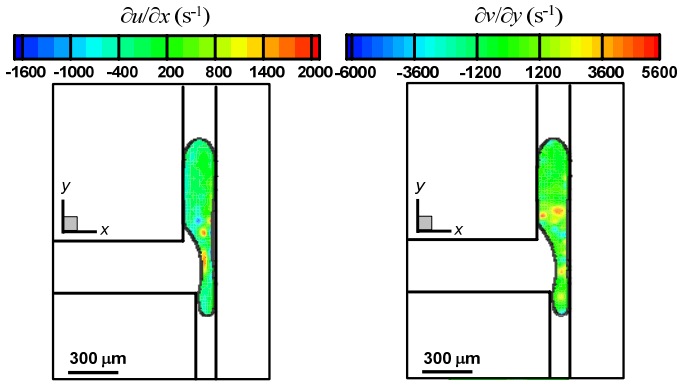

(a) (b)

Figure 8 rate of linear deformation in (a) x direction and (b) y direction, $R_1/R_2 = 0.62$, $\theta = 180°$ and $\dot{Q}_c / \dot{Q}_d = 2$, $t = 4.316$ ms

Figure 9 displays the velocity magnitude of droplet centroid in bifurcating microchannel of different θ for R_1/R_2 = 0.62. As mentioned earlier, droplet accelerates in a bifurcating microchannel of $\theta = 30°$ when it approaches the fission region. After fragmentation, the two droplet moves at a different speed, i.e. droplet in the wider channel travels faster than that in the narrower channel. For $\theta = 180°$, on the other hand, droplet drastically slows down when it enters the fission region. Unlike the case of $\theta = 30°$, no apparent increase in velocity is observed when the droplet is stretched toward the daughter channels. Another distinct characteristic is the splitting droplets move in nearly identical speed after the fission, as revealed in Fig. 9.

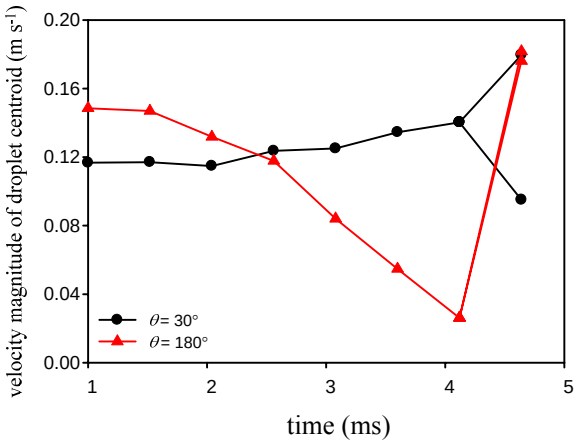

Figure 9 comparison of the velocity magnitude of droplet centroid for $R_1/R_2 = 0.62$ and $\dot{Q}_c / \dot{Q}_d = 2$

CONCLUSION

In the present work, the μPIV diagnosis is carried out to study the internal flow field of a dividing droplet in an asymmetric bifurcating microchannel. The lengths and widths of the two arms are designed so the pressure drops are identical across the two daughter channels. Besides the existence of the critical capillary number above which droplet fission is possible, there is also an upper limit of $\dot{Q}_c / \dot{Q}_d$ for bifurcating microchannel of R_1/R_2 = 0.38 and $\theta = 180°$. In an asymmetric bifurcation of $\theta = 180°$, the capillary forces become more important as branch narrows. As $\dot{Q}_c / \dot{Q}_d$ increases, the mother droplet shrinks and interfacial forces overrule flow momentum so that droplet breakup is ceased. When droplet approaches the bifurcation, the counter-rotating vortices disintegrate and a saddle point emerges. Unlike

the case of $\theta = 180°$, no evident deceleration is found for droplet in a bifurcating microchannel of $\theta = 30°$ or 60°. Instead, fluid is pulled toward the wider branch because of its lower capillary resistance and strong rotation rate of fluid is observed near the pinnacle. In bifurcating microchannel of $\theta = 180°$, on the other hand, mother droplet drastically slows down near the fission region and experiences stretches from the two opposite arms. As a result, droplet is divided into more comparable portions without the aid of a sharp edge and the two daughter droplets moves at nearly identical speed after fission. This study proves that the sharp edge actually is beneficial to droplet breakup and we are able to obtain daughter droplets of highly disproportional sizes in extremely asymmetric fork.

ACKNOWLEDGEMENT

This work is supported by the National Science Council of Taiwan under grant number NSC 101-2221-E-002-084-MY2.

REFERENCES

[1] Tan Y-C Fisher JS Lee AI Cristini V Phillip A "Design of microfluidic channel geometries for the control of droplet volume, chemical concentration, and sorting" Lab on a Chip 4 (2004) pp.292-298

[2] Nie J and Kennedy RT "Sampling from nanoliter plugs via asymmetrical splitting of segmented flow" Analytical Chemistry 82 (2010) pp.7852-7856

[3] Link DR Anna SL Weitz DA Stone HA "Geometrically mediated breakup of drops in microfluidic devices" Physical Review Letters 92 (2004) pp.054503

[4] Glawdel T Elbuken C Ren C "Passive droplet trafficking at microfluidic junctions under geometric and flow asymmetries" Lab on a Chip 11 (2011) pp.3774-3784

[5] Tan Y-C Collins J Lee AP, "Controlled fission of droplet emulsion in bifurcating microfluidic channels," in *The 12th International Conference on Solid State Sensors, Actuators, and Microsystems (Transducers'03)*. Boston, 2003, pp. 28-31.

[6] Ménétrier-Deremble L and Tabeling P "Droplet breakup in microfluidic junctions of arbitrary angles" Physical Review E 74 (2006) pp.035303

[7] Bedram A and Moosavi A "Droplet breakup in an asymmetric microfluidic T junction" The European Physical Journal E 34 (2011) pp.1-8

[8] Samie M Salari A Shafii MB "Breakup of microdroplets in asymmetric T junctions" Physical Review E 87 (2013) pp.053003

[9] Garstecki P Fuerstman MJ Stone HA Whitesides GM "Formation of droplets and bubbles in a microfluidic T-junction - scaling and mechanisms of break-up" Lab on a Chip 6 (2006) pp.437-446

[10] van Steijn V Kleijn CR Kreutzer MT "Flows around confined bubbles and their importance in triggering pinch-off" Physical Review Letters 103 (2009) pp.214501

[11] van Steijn V Kreutzer MT Kleijn CR "μ-PIV study of the formation of segmented flow in microfluidic T-junctions" Chemical Engineering Science 62 (2007) pp.7505-7514

[12] Leshansky AM and Pismen LM "Breakup of drops in a microfluidic T junction" Physics of Fluids 21 (2009) pp.023303

[13] Jullien M-C Tsang Mui Ching M-J Cohen C Lenetrier L Tabeling P "Droplet breakup in microfluidic T-junctions at small capillary numbers" Physics of Fluids 21 (2009) pp.072001

[14] Fu T Ma Y Funfschilling D Li HZ "Dynamics of bubble breakup in a microfluidic T-junction divergence" Chemical Engineering Science 66 (2011) pp.4184-4195

[15] Sessoms DA Belloul M Engl W Roche M Courbin L Panizza P "Droplet motion in microfluidic networks: Hydrodynamic interactions and pressure-drop measurements" Physical Review E 80 (2009) pp.016317

[16] Wu Y Fu T Zhu C Lu Y Ma Y Li HZ "Asymmetrical breakup of bubbles at a microfluidic T-junction divergence: feedback effect of bubble collision" Microfluidics and Nanofluidics 13 (2012) pp.723-733

[17] Ryerson WG and Schwenk K "A simple, inexpensive system for digital particle image velocimetry (DPIV) in biomechanics" Journal of Experimental Zoology Part A: Ecological Genetics and Physiology 317 (2012) pp.127-140

[18] Schneider CA Rasband WS Eliceiri KW "NIH Image to ImageJ: 25 years of image analysis" Nature Methods 9 (2012) pp.671-675

[19] White FM "Viscous Fluid Flow", 3rd edn. McGraw-Hill (2006)

[20] Kinoshita H Kaneda S Fujii T Oshima M "Three-dimensional measurement and visualization of internal flow of a moving droplet using confocal micro-PIV" Lab on a Chip 7 (2007) pp.338-346

[21] Bretherton FP "The motion of long bubbles in tubes" Journal of Fluid Mechanics 10 (1961) pp.166-188